Applied Surface Science 529 (2020) 147168

Contents lists available at ScienceDirect

Applied Surface Science

journal homepage: www.elsevier.com/locate/apsusc

Non-axial N_O-V_{Zn} shallow acceptor complexes in nitrogen implanted *p*-type ZnO thin films

Wanjun Li[a], Hong Zhang[a,*], Xiaoyu Zhang[a], Guoping Qin[a], Honglin Li[a], Yuanqiang Xiong[a], Lijuan Ye[a], Haibo Ruan[c], Cunzhu Tong[d], Chunyang Kong[a], Liang Fang[b,*]

[a] Chongqing Key Laboratory of Photo-Electric Functional Materials, College of Physics and Electronic Engineering, Chongqing Normal University, Chongqing 401331, PR China

[b] State Key Laboratory of Power Transmission Equipment & System Safety and New Technology, Chongqing Key Laboratory of Soft Condensed Matter Physics and Smart Materials, College of Physics, Chongqing University, Chongqing 400044, PR China

[c] Research Center for Materials Interdisciplinary Sciences, Chongqing University of Arts and Sciences, Chongqing 402160, PR China

[d] State Key Laboratory of Luminescence and Applications, Changchun Institute of Optics, Fine Mechanics and Physics, Chinese Academy of Sciences, No. 3888 Dong Nanhu Road, Changchun, Jilin 130033, PR China

ARTICLE INFO

Keywords:
ZnO films
N-doping
p-Type
Post-annealing
Shallow acceptor complex

ABSTRACT

Over the past two decades, there have been numerous reports about the *p*-type behavior of N-doped ZnO. To date, however, its origin still remains mysterious, especially, N ion-implanted ZnO system. Herein, ZnO films were implanted with 70 keV N ions to a fluence of 1×10^{17} cm^{-2} at room temperature, followed by annealing in the range of 750–950 °C. The obtained *p*-type ZnO films have a widely hole concentration of $2.87 \times 10^{15} \sim 2.64 \times 10^{16}$ cm^{-3}, a mobility of $1.37 \sim 7.27$ cm^{2}V^{-1}s^{-1} and a resistivity of $148.3 \sim 299.4$ Ω.cm. The thermal evolution of point defects and the possible shallow acceptors in N-implanted ZnO films were further investigated by means of Raman scattering, Photoluminescence (PL) and Electron paramagnetic resonance (EPR). The results show that abundant intrinsic-related defects including zinc interstitials (Zn_i), oxygen vacancies (V_O) and zinc vacancies (V_{Zn}) were introduced during ion implantation. It is demonstrated that appropriate post-annealing can not only reduce the compensation of donor defects, but also facilitate the formation of N-related shallow acceptor complexes, both of which contribute to the *p*-type conduction transition of N-implanted ZnO films. The *non-axial* N_O-V_{Zn} complexes are proposed to be a kind of potential and stable acceptors in N ion-implanted ZnO films.

1. Introduction

Zinc oxide, as a fascinating wide direct band gap semiconductor with a large free-exciton binding energy of 60 meV, is considered a very promising material for next generation short-wavelength optoelectronic devices, such as light emitting diodes (LEDs), laser diodes (LDs), and ultraviolet (UV) detectors [1,2]. Unfortunately, the emergence of such novel optoelectronic devices suffers from the lack of easily available *p-n* homojunctions. Until now, highly efficient *p*-type doping remains a great challenge due to the strong self-compensation effect, low solubility of acceptors, and deep acceptor levels in ZnO [2]. Nevertheless, some highlights are presented by researchers over the past decade. For example, the first room temperature violet electroluminescence from the *p-i-n* homojunctions based on Nitrogen-doped ZnO has been demonstrated by Tsukazaki et al. [3]. After that, Liu et al. realized highly stable room temperature electrically pumped laser diodes that consist of Sb-doped *p*-type ZnO nanowires and n-type ZnO films [4]. Recently, Shen et al. developed dynamic N doping technology and the corresponding ZnO-based *p-i-n* homojunctions can work continuously for over 300 h at room temperature [5]. These encouraging results, but far from these, demonstrate that *p*-type doping for ZnO is feasible [2].

Highly efficient *p*-type doping requires both the formation of sufficient shallow acceptor and the suppression of donor compensation. Among potential acceptor dopants, the substitution of nitrogen for oxygen (N_O) has been considered as the most suitable method for generating hole carriers, stemming from their similar atomic size and electronic structure. Experimentally, the obtained values of acceptor ionization energy for N-doped ZnO are mainly distributed in the range of 160 ± 40 meV via photoluminescence measurements [6–11]. So, N_O acceptors were once thought to be the hole origin of *p*-type N-doped

* Corresponding authors.
E-mail addresses: zhh_2016@163.com (H. Zhang), lfang@cqu.edu.cn (L. Fang).

https://doi.org/10.1016/j.apsusc.2020.147168
Received 10 June 2020; Received in revised form 1 July 2020; Accepted 3 July 2020
Available online 08 July 2020

ZnO, until J.L. Lyons et al. revisited the properties of N in ZnO by the first-principles based on the hybrid functional. They found that isolated N_O were deep acceptors with an exceedingly high ionization energy of 1.3 eV, far exceeding the experimental value [12]. Subsequently, further theoretical and experimental studies also supported their results [13–15]. Hence, the *p*-type conductivity in the N-doped ZnO is probably not from the isolated N_O defects but from N-related derivative complexes. At present, some complex acceptor models have been proposed but still lack further experimental verification [16–19]. Especially, the axial N_O-V_{Zn} shallow acceptor model proposed by Liu et al. has attracted great attention from researchers [16]. They found that the metastable axial N_{Zn}-V_O double donor can be favored by the Zn-polar growth and convert into axial N_O-V_{Zn} shallow acceptor via overcoming an energy barrier of about 1.1 eV. Inspired by the work of Liu et al., Reynolds et al. reported the *p*-type ZnO:N films with the hole concentration of 10^{18} cm^{-3} on a sapphire substrate by organometallic vapor phase epitaxy, the *p*-type behavior of which was attributed to V_{Zn}-N_O-H^+ shallow acceptor complex [7], but lack of follow-up work. It should be mentioned that the key point for the formation of the above shallow acceptor complexes is the requirement of the Zn polar growth surface. Actually, not all *p*-type N-doped ZnO is prepared on the Zn-polar surface, such as N-ion implantation [20,21]. Furthermore, Yong et al. revealed that the energy of *non-axial* N_O-V_{Zn} complex is lower by about 0.06 eV than that of axial N_O-V_{Zn} complex, and the hydrogenation of N_O can greatly enhance the binding between N_O and V_{Zn} [18]. Therefore, the origin of the *p*-type conductivity in N-doped ZnO remains to be mysterious, and the microstructure of the acceptors themselves and their formation need more research.

In this work, we investigated the thermal evolution of defects and the transformation mechanism of *p*-type conductivity in N-implanted ZnO films combined with the measurements of Raman-scattering, Photoluminescence and Electron paramagnetic resonance. The *non-axial* N_O-V_{Zn} complexes are proposed to be a potential shallow acceptor for *p*-type N-implanted ZnO films.

2. Material and methods

N-doped ZnO films were prepared by following procedure. Firstly, undoped ZnO films with a thickness of about 400 nm were deposited at room temperature on quartz substrates (5 × 5 mm^2) using radio frequency magnetron sputtering system (JGP-450, SKY Technology Development Co., Ltd, China) by utilizing a commercial ZnO ceramic target supplied by China New Metal Materials Technology Co., Ltd. The sputtering chamber was evacuated to a base pressure of 5 × 10^{-4} Pa with a turbo molecular pump. During the sputtering, the flow rate of Ar (99.999%) was fixed at 40 sccm. Moreover, the sputtering time, power and pressure were maintained at 35 min, 120 W and 1 Pa, respectively. Secondly, the as-deposited ZnO films were subjected to N ion implantation with the energy of 70 keV and a dose of 1 × 10^{17} cm^{-2}. Subsequently, as-implanted ZnO:N films, which behave high resistance state, undergo a rapid thermal annealing in the tubular furnace to activate acceptor defects and repair lattice damage. Specifically, the films were annealed rapidly for 5 min at different temperatures (750, 800, 850, 900 and 950 °C) and high purity N_2 was used as the protective gas.

The electrical properties of the samples were evaluated at room temperature (RT) by a Hall Effect measurement system (HMS-3000, Ecopia). The structural properties of the samples were characterized by X-ray diffraction (PANalytical X'Pert Powder) equipped with high-intensity Cu Kα_1 radiation (λ = 0.15418 nm). Raman scattering spectra were recorded at RT on a JY Horiba LabRam HR spectrometer with the 532 nm excitation laser. Photoluminescence spectra of the samples were acquired by exciting with a 325 nm He-Cd laser at both RT and 4 K. Electron paramagnetic resonance (EPR) measurements were carried out at 77 K using a Jeol JES-FA-200 spectrometer operating near ~9.07 GHz (0.98 mW microwave power). And a 100 W xenon lamp served as an excitation source for photo-excitation EPR (photo-EPR) measurements. X-ray photoelectron spectroscopy (XPS, Thermo ESCALAB 250) measurements were carried out to study the chemical states of N-dopants using a monochromatic Al K_α source (15 kV, 150 W) and all binding energies have been calibrated by the C 1*s* peak at 284.6 eV.

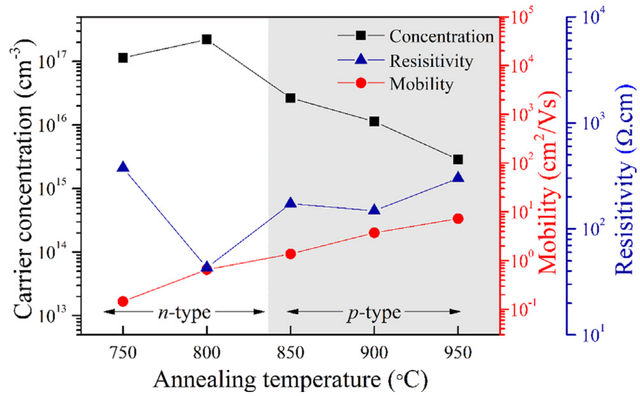

Fig. 1. Room temperature electrical properties of annealed ZnO:N films.

3. Results and discussion

Room temperature electrical properties of N-doped ZnO films annealed at various temperature ranging from 750 to 950 °C for 5 min are shown in Fig. 1. The films annealed at 750 ~ 800 °C did not directly convert to *p*-type, but show a good *n*-type conductivity with the electron concentration of ~10^{17} cm^{-3} possibly due to the low acceptor defect concentration and the serious compensation from the intrinsic donor defects. Noted that the films achieve *p*-type conductivity when the annealing temperature up to 850 °C, and the corresponding hole concentration, mobility and resistivity are 2.64 × 10^{16} cm^{-3}, 1.37 $cm^2V^{-1}s^{-1}$ and 172.6 Ω.cm, respectively, similar to the results achieved by Xie et al. [5]. With the increase of annealing temperature, the films still show *p*-type conductivity, but the hole concentration monotonically decreases from 2.64 × 10^{16} cm^{-3} to 2.87 × 10^{15} cm^{-3}, as shown in Fig. 1. From the Hall measurement, it can be seen that rapid thermal annealing at 850 ~ 950 °C has the ability to activate sufficient acceptor defects or eliminate partial donor-type compensation defects, making the acceptor become predominant in the films. Especially, annealing at 850 °C favors to obtain *p*-type ZnO:N films with good electrical properties. These results demonstrated that the N ions implantation method is an effective approach to achieve *p*-type ZnO:N films.

To evaluate the crystalline quality and the change in the local structure, defect states or disorder in the ZnO:N films, Raman scattering studies were performed. Fig. 2(a) shows the Raman spectra of as-implanted and annealed ZnO:N films. It can be clearly seen that they all exhibit the E_2(low), E_2(M), E_2(high) and A_1(LO) vibrational modes of typical wurtzite ZnO, located at ~99, ~333, ~437 and ~580 cm^{-1}, respectively. In addition, three additional Raman modes, located at ~275 cm^{-1} (P_1), ~510 cm^{-1} (P_2) and ~640 cm^{-1} (P_3), are also observed in all ZnO:N films. The E_2(low) and E_2(high) modes are related to the vibration of lattice O and lattice Zn in ZnO, respectively, of which the intensity strongly depends on the crystal quality of films. As is shown in Fig. 2(b), the intensities of both E_2(low) and E_2(high) mode increase first and then decreases slightly with annealing temperature, indicating that thermal annealing at proper temperature can effectively improve the crystal quality of ZnO:N thin films. The above result was also further confirmed by XRD measurements, as shown in Fig. S1 of Supplementary Material. The A_1(LO) vibration mode is generally related to intrinsic defects (Zn_i, V_O) or their complex in ZnO, while three additional modes are often induced by N doping. Noted that the ~275 cm^{-1} (P_1) mode has been recently attributed to the Zn_i related shallow donors in ZnO:N films [22–24]. As shown in Fig. 2(a), as-

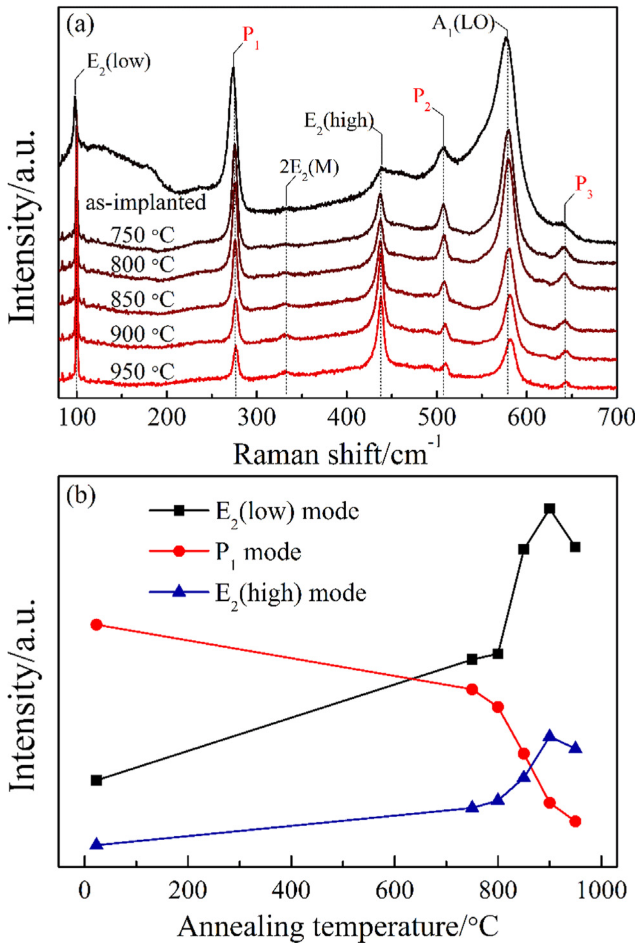

Fig. 2. (a) Raman spectra of as-implanted and annealed ZnO:N films; (b) The extracted intensities of E_1(low), 275 cm^{-1}(P_1) and E_2(high) modes.

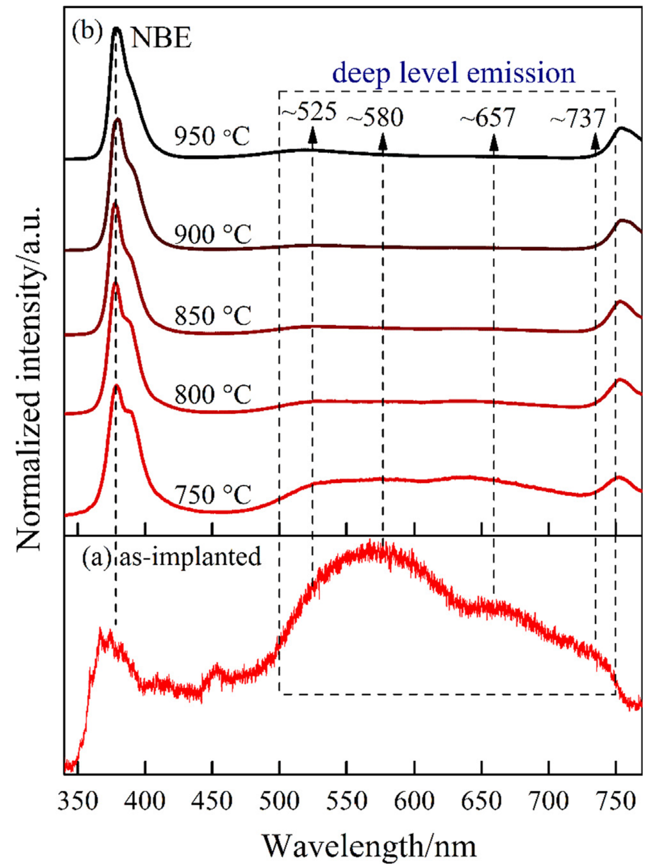

Fig. 3. The normalized room temperature PL spectra: (a) as-implanted ZnO:N film; (b) annealed ZnO:N films.

implanted ZnO:N film shows the prominent P_1 and A_1(LO) vibration modes under the action of ion bombardment. After high-temperature rapid annealing, their intensities decrease significantly, which indicates the concentration of intrinsic donor defects (Zn_i, V_O) created by implantation can be effectively suppressed by high-temperature rapid annealing treatment.

Room temperature photoluminescence (PL) spectra have been employed to further investigate the influence of ion implantation and rapid annealing treatment on intrinsic defects in ZnO:N films and the results are shown in Fig. 3. It is generally known that ion implantation process will induce a large number of crystal defects and non-radiative recombination centers. As the potential trap centers, they directly cause the near-band-edge emission (NBE) peak (~375 nm) of as-implanted ZnO:N film to exhibit a weak luminescence intensity and a large full width at half maximum, while the deep level emission band in the visible region of 500–750 nm dominates the entire spectrum of as-implanted ZnO:N film, as shown in Fig. 3(a). The yellow-green emission between 500 and 600 nm is usually attributed to the oxygen vacancy related defects, involving V_O^+ (~525 nm) and V_O^{2+} (~580 nm) [25]. The red excitation consists of two components: ~657 nm (~1.89 eV) and ~737 nm (~1.68 eV). In the electron irradiated samples, Knutsen et al. claimed the characteristic red emission at ~680 nm (~1.75 eV) was associated with the optical transition involving zinc vacancy (V_{Zn}) related deep acceptors and shallow donors (possibly including Zn_i) based on PL spectra and positron annihilation spectroscopy (PAS) [26]. In addition, Dong et al. found that the observed red excitation can be deconvolved into peaks at ~1.6 and ~1.9 eV with pronounced defect emission at 1.6 eV in N-implanted ZnO [27]. The former involves isolated V_{Zn} emission while the latter is related to the transition between conduction band and the energy level of V_{Zn} related clusters [27]. In this work, our experimental results are very conformable to that of Dong et al.. Hence, the observed 657 nm red excitation could be conformed to V_{Zn} related clusters and later one (737 nm) is close to the isolated V_{Zn}. Besides, two additional blue emissions (~413 nm and ~453 nm) can be distinguished in as-implanted films, which have been attributed to the optical transitions from Zn_i and extended Zn_i states to the valance band, respectively [28]. Hence, room temperature PL spectra revealed that the N ion implantation process indeed induces rich donor defects (Zn_i, V_O) and V_{Zn}-related defects.

To shed more light on the variation of these intrinsic defects with annealing temperature, all spectra of annealed ZnO:N films are normalized to the NBE peaks, as shown in Fig. 3(b). Obviously, annealing treatment promotes the NBE peaks become very sharp peak and even dominate the entire PL spectra, confirming that post-annealing can effectively eliminate abundant non-radiative recombination centers by improving the crystal quality of films. The weak emission feature near 753 nm is due to the second order contribution of the strong NBE emission. At the same time, the intensity of deep level emission band (V_O, V_{Zn}, and V_{Zn} clusters) decreases significantly with the annealing temperature. In particular, the intensity of V_O-related yellow-green emission has a great decline and the isolated V_{Zn} emission at 737 nm disappeared after annealing. However, it can be found that the intensity of V_O^+ related emission at ~525 nm appears to slightly increase when the annealing temperature up to 950 °C, implying that the V_O donor defects will be induced again under the condition of excessively high temperature.

It is noteworthy that high temperature annealing has the ability to lead to the dissociation of Zn_i-related defects to form migratable isolated Zn_i defects. Under the action of thermal energy, some isolated Zn_i

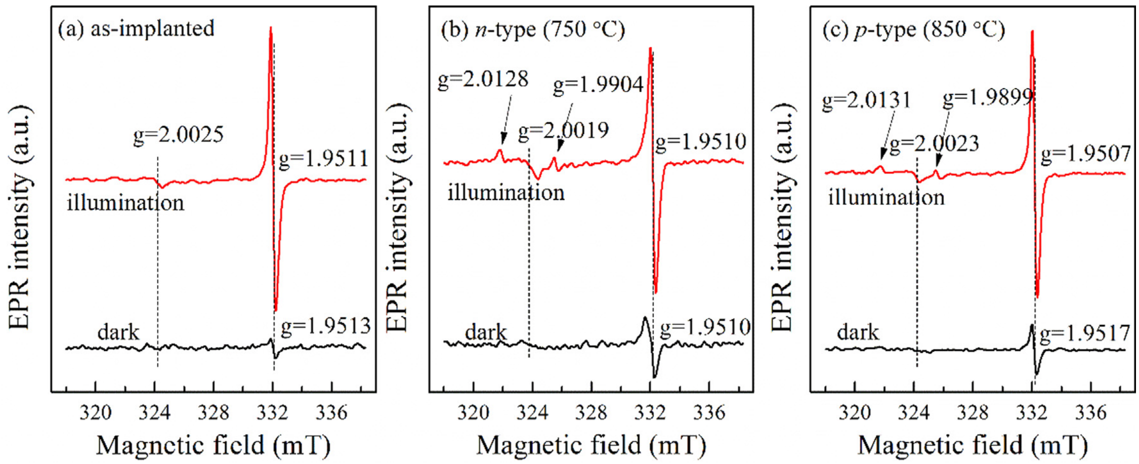

Fig. 4. EPR spectra before and after an exposure to xenon lamp light at 77 K: (a) as-implanted sample, (b) *n*-type (750 ˚C), and (c) *p*-type (850 ˚C). The external magnetic field is perpendicular to the substrates.

defects will diffuse out of the films or migrate into the lattice position, which may be an important reason for the quenching of the blue emission, in agreement with the report by Zeng et al. [28]. Meanwhile, a shoulder at ~389 nm (3.19 eV) emerged at the lower energy side of NBE after annealing, which has been indexed to the transition from shallow donor defects to valence band maximum [29], especially from the residual Zn_i defects [30,31]. The intensity of shoulder gradually decreases with annealing, which is consistent with the decrease of Zn_i defect concentration. Overall, both Raman and PL measurements revealed that appropriate thermal treatment effectively reduced the concentration of related donor compensating defects (V_O and Zn_i), which is advantageous for the *p*-type conductivity transition of the ZnO:N films.

To understand the formation mechanism of *p*-type conductivity in ZnO:N films, we will focus on three representative samples, including as-implanted, *n*-type (750 ˚C) and *p*-type (850 ˚C) ZnO:N films. EPR is a powerful tool for monitoring the defects with unpaired electrons, particularly vacancy defects. Fig. 4 shows the EPR spectra of three representative samples before and after an exposure to xenon lamp light at 77 K. Only one resonance signal near 332 mT ($g_{||} = 1.9510$) can be observed in all spectra in the dark, prior to illumination by a xenon lamp. This resonance signal is associated with shallow donors, likely Zn_i-related defects [28]. After illumination, shallow donor signal is enhanced, accompanied by the emergence of new resonance signals located at 322, 324, and 326 mT, respectively. The new resonance signal at ~326 mT ($g_{||} = 1.9904$), involving singly ionized oxygen vacancy (V_O^+) defects [32,33], can be observed at annealed samples (750 ˚C and 850 ˚C), as shown in Fig. 4(b-c). In the early literature, the signal at ~324 mT ($g_{||} =$ ~2.0025) was reported in the electron irradiated ZnO single crystals, which are attributed to axial V_{Zn} defects [34,35]. Recently, Holston et al. also observed a similar photo-EPR signal in neutron irradiated ZnO crystals and attributed it to the $(V_O^{2+}$-$V_{Zn}^-)^+$ divacancy [36]. Considering that the red excitation associated with V_{Zn} related clusters still exists and the isolated V_{Zn} related excitation peak disappeared after annealing, we are inclined to attribute the signal at ~324 mT ($g_{||} =$ ~2.0025) to V_O-V_{Zn} divacancy. Actually, the formation of V_O-V_{Zn} divacancy has been discovered in different experimental conditions, such as irradiation, annealing and polishing [36–38]. Especially, the N ion implantation can induce a large number of V_{Zn} and V_O defects, creating an effective condition for the formation of V_O-V_{Zn} clusters [37]. Theoretically, the V_O-V_{Zn} clusters can exist in two different configurations, axial (aligned along the [0001] direction) and non-axial (lying in the basal plane) [36]. However, theoretical calculation indicate that the non-axial configuration is more stable [39,40], which should be the primary divacancy in the films. It is recently reported that $(V_O^{2+}$-$V_{Zn}^-)^+$ clusters is in a paramagnetic state (S = 1/2) with a similar electron structure of V_{Zn}^-, and the unpaired spinning electron mainly existed in one of the three O ions adjacent to V_{Zn} [39]. Bang et al. investigated that the growth and stability of V_O-V_{Zn} clusters by kinetic Monte Carlo simulation [40]. They found that the cluster has a large dissociation energy over 2.5 eV, which explains why the signal still existed in the annealed samples.

More interestingly, the annealed samples show the additional EPR signal at 322 mT ($g_{||} = 2.0128$) due to non-axial V_{Zn} defects [41,42], where the holes are localized at non-axial anions. This means that the local environment around V_{Zn} has changed after post-annealing [43]. The possible reason is that the non-axial anion sites adjacent to V_{Zn} have elements other than oxygen, most likely N elements. Furthermore, the XPS measurements are utilized to examine the chemical state of N elements in films. The peak centered near the binding energy of ~396 eV is ascribed to nitrogen on oxygen sites (N_O) (Fig. S2, Supplementary material), supporting the conjecture that the non-constituent element should be nitrogen. Recently, Yong et al. revealed that the energy of non-axial N_O-V_{Zn} cluster is lower by about 0.06 eV than that of axial N_O-V_{Zn} cluster [18]. At the same time, they also pointed out that the formation of non-axial N_O-V_{Zn} clusters may result from the migration of V_{Zn} and then recombination with a neighboring N_O defect. For this reason, it is highly likely that non-axial N_O-V_{Zn} acceptor complexes are formed during annealing. The corresponding model of non-axial N_O-V_{Zn} cluster is shown in the inset of Fig. 5(b). It should be emphasized that post-annealing also provides opportunities for the recombination of non-axial V_O-V_{Zn} and nearby N atoms to form non-axial N_O-V_{Zn} complexes. However, more detailed defect formation behavior needs further study.

For getting more optical information about nitrogen acceptor in ZnO:N films, Fig. 5(a) compares the 4 K low-temperature photoluminescence (PL) spectra of *n*-type (750 ˚C) and *p*-type (850 ˚C) samples. As plotted in Fig. 5(a), the dominant PL peak for *p*-type (850 ˚C) sample is the neutral acceptor bound exciton (A^0X) transition at 3.360 eV, and the neutral donor bound exciton (D^0X) peak is at 3.369 meV, consistent with the results of Huang et al. [11]. The peak at 3.311 eV is due to the free electron-to acceptor (FA) transition [9], which has been observed previously in ZnO doped with P [44], As [45] and Sb [46]. The donor–acceptor pair (DAP) transition appeared at 3.233 eV, accompanying with the first-order longitudinal optical (LO) phonon replica lines centered at 3.161 eV. Similarly, the PL spectrum for *n*-type one (750 ˚C) also contains DAP, FA and A^0X peaks, but their intensities were significantly less than that of the *p*-type sample. In addition, the spectrum of *n*-type ZnO:N is dominated by the familiar deeply donor bound exciton (Y_0 line) at 3.336 eV, accompanying with

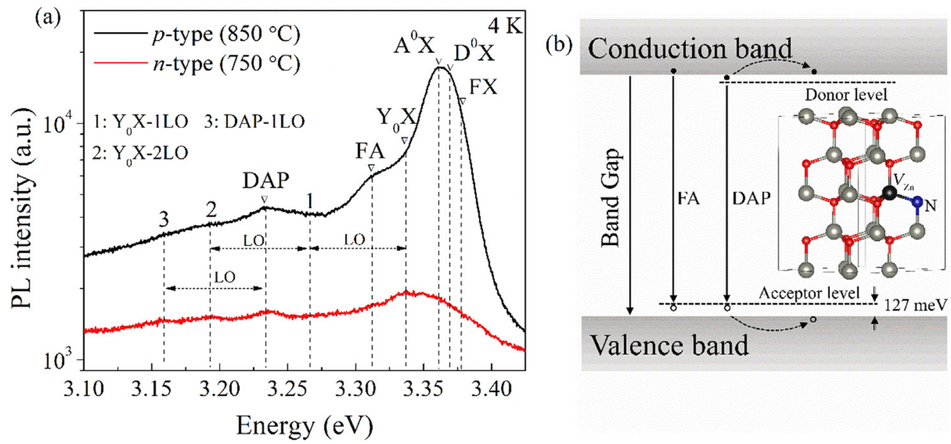

Fig. 5. (a) 4 K low-temperature PL of ZnO:N films; (b) schematic diagram of the energy levels. The inset shows the model of non-axial N_O-V_{Zn} acceptor complex.

two LO phonon replicas lines centered at 3.266 and 3.194 eV, respectively. The Y line originates from the radiative recombination of excitons bound to extended structural defect complexes [47]. The extended structural defects are most likely due to stacking faults induced by N ion implantation [48]. A weak Y^0 line can still be observed after annealing at 850 °C, indicating that it is difficult to completely eliminate these structural defects by annealing. As we all know, the acceptor binding energy (E_A) in ZnO can be estimated by the following formula [10,49,50]:

$$E_A = E_g - E_{FA} + \frac{1}{2}k_B T \quad (1)$$

where E_g, E_{FA}, K_B and T are the intrinsic band gap energy of ZnO (E_g = 3.437 eV), the free electron to acceptor energy, the Boltzmann constant, and the temperature, respectively. The estimated acceptor binding is about 127 meV by formula (1), in good agreement with the current experimental value of 160 ± 40 meV in the single N-doped ZnO system [6–11]. The corresponding schematic diagram of the energy levels is shown in Fig. 5(b). Therefore, the non-axial N_O-V_{Zn} cluster should be an important shallow acceptor complex for *p*-type ZnO:N films.

Based on the above discussion, the formation mechanism of *p*-type conductivity in N-implanted ZnO films can be explained well as following: (i) Abundant defects (V_{Zn}, V_O-V_{Zn}, N_O) induced by N ion implantation provide opportunities for the construction of N-related shallow acceptor complexes; (ii) Appropriate post-annealing treatment not only favors the formation of sufficient non-axial N_O-V_{Zn} shallow acceptor defects but also reduces the compensation of donor defects (V_O, Zn_i), resulting in that the conductivity of the ZnO:N film converts from *n*-type to *p*-type; (iii) Excessive annealing temperature encourages the out-diffusion of N-dopants (Fig. S2), leading to decrease in the hole concentration of the *p*-type ZnO:N films. Therefore, optimizing annealing conditions may further improve the conductivity properties of *p*-type ZnO:N films.

4. Conclusion

In summary, *p*-type ZnO:N films have been realized by ion implantation and post-annealing, the electrical properties of which strongly depend on annealing temperature. The ZnO:N films are *n*-type at the annealing temperatures of 750 and 800 °C, but convert to *p*-type after 850 °C due to the formation of sufficient acceptor defects and the elimination of donor-type compensation defects. Further increasing annealing temperature, the films still show *p*-type conduction, but the hole concentration monotonically decreases. The corresponding shallow acceptors have been identified as non-axial N_O-V_{Zn} shallow acceptor complex, possibly from the recombination between N_O and V_{Zn} or V_O-V_{Zn} divacancy during annealing. Therefore, an appropriate design to intentionally induce non-axial N_O-V_{Zn} complex and suppress intrinsic donor defects in N-doped ZnO film might be is a possible way to achieve reliable *p*-type ZnO materials. We also hope that this study will motivate more experimental and theoretical efforts to reveal more detailed information for the non-axial N_O-V_{Zn} acceptor complex.

CRediT authorship contribution statement

Wanjun Li: Methodology, Writing - original draft. **Hong Zhang:** Conceptualization, Writing - review & editing. **Xiaoyu Zhang:** Investigation, Validation. **Guoping Qin:** Methodology, Data curation. **Honglin Li:** Visualization, Methodology. **Yuanqiang Xiong:** Visualization. **Lijuan Ye:** Visualization. **Haibo Ruan:** Validation. **Cunzhu Tong:** Resources, Funding acquisition. **Chunyang Kong:** Supervision, Funding acquisition. **Liang Fang:** Writing - review & editing, Funding acquisition.

Declaration of Competing Interest

The authors declare that they have no known competing financial interests or personal relationships that could have appeared to influence the work reported in this paper.

Acknowledgments

This work was supported by the National Natural Science Foundation of China (Grant No. 51472038, 11904041, 11747146), the Natural Science Foundation of Chongqing (Grant No. cstc2019jcyjmsxmX0237, cstc2018jcyjA2923), the Science and Technology Research Project of Chongqing Education Committee (Grant No. KJ1703042, KJ1500319), the State Key Laboratory of Luminescence and Applications (SKLA-2020-10), and the Dr. Scientific Research Fund of Chongqing normal university (Grant No. 20XlB002).

Appendix A. Supplementary data

Supplementary data to this article can be found online at https://doi.org/10.1016/j.apsusc.2020.147168.

References

[1] A. Janotti, C.G. Van de Walle, Fundamentals of zinc oxide as a semiconductor, Rep. Prog. Phys. 72 (2009) 126501, , https://doi.org/10.1088/0034-4885/72/12/126501.
[2] J.C. Fan, K.M. Sreekanth, Z. Xie, S.L. Chang, K.V. Rao, p-Type ZnO materials: theory, growth, properties and devices, Prog. Mater Sci. 58 (2013) 874–985, https://doi.org/10.1016/j.pmatsci.2013.03.002.
[3] A. Tsukazaki, A. Ohtomo, T. Onuma, M. Ohtani, T. Makino, M. Sumiya, K. Ohtani,

S.F. Chichibu, S. Fuke, Y. Segawa, H. Ohno, H. Koinuma, M. Kawasaki, Repeated temperature modulation epitaxy for p-type doping and light-emitting diode based on ZnO, Nat. Mater. 4 (2005) 42–46, https://doi.org/10.1038/nmat1284.

[4] S. Chu, G.P. Wang, W.H. Zhou, Y.Q. Lin, L. Chernyak, J.Z. Zhao, J.Y. Kong, L. Li, J.J. Ren, J.L. Liu, Electrically pumped waveguide lasing from ZnO nanowires, Nat. Nanotechnol. 6 (2011) 506–510, https://doi.org/10.1038/NNANO.2011.97.

[5] X.H. Xie, B.H. Li, Z.Z. Zhang, D.Z. Shen, Reinventing a p-type doping process for stable ZnO light emitting devices, J. Phys. D: Appl. Phys. 51 (2018) 225104, , https://doi.org/10.1088/1361-6463/aabe49.

[6] J.E. Stehr, X.J. Wang, S. Filippov, S.J. Pearton, I.G. Ivanov, W.M. Chen, I.A. Buyanova, Defects in N, O and N, Zn implanted ZnO bulk crystals, J. Appl. Phys. 113 (2013) 103509, , https://doi.org/10.1063/1.4795261.

[7] J.G. Reynolds, C.L. Reynolds, A. Mohanta, J.F. Muth, J.E. Rowe, H.O. Everitt, D.E. Aspnes, Shallow acceptor complexes in p-type ZnO, Appl. Phys. Lett. 102 (2013) 152114, , https://doi.org/10.1063/1.4802753.

[8] D.C. Look, D.C. Reynolds, C.W. Litton, R.L. Jones, D.B. Eason, G. Cantwell, Characterization of homoepitaxial p-type ZnO grown by molecular beam epitaxy, Appl. Phys. Lett. 81 (2002) 1830–1832, https://doi.org/10.1063/1.1504875.

[9] J.W. Sun, Y.M. Lu, Y.C. Liu, D.Z. Shen, Z.Z. Zhang, B. Yao, B.H. Li, J.Y. Zhang, D.X. Zhao, X.W. Fan, Nitrogen-related recombination mechanisms in p-type ZnO films grown by plasma-assisted molecular beam epitaxy, J. Appl. Phys. 102 (2007) 043522, , https://doi.org/10.1063/1.2772581.

[10] M. Ding, D.X. Zhao, B. Yao, B.H. Li, Z.Z. Zhang, D.Z. Shen, The p-type ZnO film realized by a hydrothermal treatment method, Appl. Phys. Lett. 98 (2011) 062102, , https://doi.org/10.1063/1.3549304.

[11] J. Huang, S. Chu, J.Y. Kong, L. Zhang, C.M. Schwarz, G.P. Wang, L. Chernyak, Z.H. Chen, J.L. Liu, ZnO p–n Homojunction Random Laser Diode Based on Nitrogen-Doped p-type Nanowires, Adv. Opt. Mater. 1 (2013) 179–185, https://doi.org/10.1002/adom.201200062.

[12] J.L. Lyons, A. Janotti, C.G. Van de Walle, Why nitrogen cannot lead to p-type conductivity in ZnO, Appl. Phys. Lett. 95 (2009) 252105, , https://doi.org/10.1063/1.3274043.

[13] S. Lany, A. Zunger, Generalized Koopmans density functional calculations reveal the deep acceptor state of N_O in ZnO, Phys. Rev. B 81 (2010) 205209, , https://doi.org/10.1103/PhysRevB.81.205209.

[14] J. Yu, L.K. Wagner, E. Ertekin, Fixed-node diffusion Monte Carlo description of nitrogen defects in zinc oxide, Phys. Rev. B 95 (2017) 075209, , https://doi.org/10.1103/PhysRevB.95.075209.

[15] M.C. Tarun, M.Z. Iqbal, M.D. McCluskey, Nitrogen is a deep acceptor in ZnO, Aip Adv. 1 (2011) 022105, , https://doi.org/10.1063/1.3582819.

[16] L. Liu, J.L. Xu, D.D. Wang, M.M. Jiang, S.P. Wang, B.H. Li, Z.Z. Zhang, D.X. Zhao, C.X. Shan, B. Yao, D.Z. Shen, *p*-Type conductivity in N-doped ZnO: the role of the N_{Zn}-V_O complex, Phys. Rev. Lett. 108 (2012) 215501, , https://doi.org/10.1103/PhysRevLett.108.215501.

[17] W.R.L. Lambrecht, A. Boonchun, Identification of a N-related shallow acceptor and electron paramagnetic resonance center in ZnO: N_2^+ on the Zn site, Phys. Rev. B 87 (2013) 195207, , https://doi.org/10.1103/PhysRevB.87.195207.

[18] D.Y. Yong, H.Y. He, Z.K. Tang, S.H. Wei, B.C. Pan, H-stabilized shallow acceptors in N-doped ZnO, Phys. Rev. B 92 (2015) 235207, , https://doi.org/10.1103/PhysRevB.92.235207.

[19] J. Bang, Y.Y. Sun, D. West, B.K. Meyer, S.B. Zhang, Molecular doping of ZnO by ammonia: a possible shallow acceptor, J. Mater. Chem. C 3 (2015) 339–344, https://doi.org/10.1039/C4TC02209B.

[20] M.A. Myers, M.T. Myers, M.J. General, J.H. Lee, L. Shao, H. Wang, P-type ZnO thin films achieved by N^+ ion implantation through dynamic annealing process, Appl. Phys. Lett. 101 (2012) 112101, , https://doi.org/10.1063/1.4751467.

[21] Q.L. Gu, C.C. Ling, G. Brauer, W. Skorupa, Y.F. Hsu, A.B. Djurišić, C.Y. Zhu, S. Fung, L.W. Lu, Deep level defects in a nitrogen-implanted ZnO homogeneous p-n junction, Appl. Phys. Lett. 92 (2008) 222109, , https://doi.org/10.1063/1.2940204.

[22] P. Zhang, C.Y. Kong, W.J. Li, G.P. Qin, Q. Xu, H. Zhang, H.B. Ruan, Y.T. Cui, L. Fang, The origin of the$\sim$ 274 cm^{-1} additional Raman mode induced by the incorporation of N dopants and a feasible route to achieve p-type ZnO: N thin films, Appl. Surf. Sci. 327 (2015) 154–158, https://doi.org/10.1016/j.apsusc.2014.11.147.

[23] H. Zhang, C.Y. Kong, W.J. Li, G.P. Qin, M. Tan, H.B. Ruan, L. Fang, Fabrication and characterization of p-type In–N codoped ZnMgO films, J. Mater. Sci. - Mater. Electron. 28 (2017) 9316–9321, https://doi.org/10.1007/s10854-017-6669-0.

[24] Z. Huang, H.B. Ruan, H. Zhang, D.P. Shi, W.J. Li, G.P. Qin, F. Wu, L. Fang, C.Y. Kong, Investigation on the p-type formation mechanism of nitrogen ion implanted ZnO thin films induced by rapid thermal annealing, Opt. Mater. Express 9 (2019) 3098–3108, https://doi.org/10.1364/OME.9.003098.

[25] P. Zhan, W.P. Wang, C. Liu, Y. Hu, Z.C. Li, Z.J. Zhang, P. Zhang, B.Y. Wang, X.Z. Cao, Oxygen vacancy–induced ferromagnetism in un-doped ZnO thin films, J. Appl. Phys. 111 (2012) 033501, , https://doi.org/10.1063/1.3679560.

[26] K.E. Knutsen, A. Galeckas, A. Zubiaga, F. Tuomisto, G.C. Farlow, B.G. Svensson, A.Y. Kuznetsov, Zinc vacancy and oxygen interstitial in ZnO revealed by sequential annealing and electron irradiation, Phys. Rev. B 86 (2012) 121203, , https://doi.org/10.1103/PhysRevB.86.121203.

[27] Y.F. Dong, F. Tuomisto, B.G. Svensson, A.Y. Kuznetsov, L.J. Brillson, Vacancy defect and defect cluster energetics in ion-implanted ZnO, Phys. Rev. B 81 (2010) 081201, , https://doi.org/10.1103/PhysRevB.81.081201.

[28] H.B. Zeng, G.T. Duan, Y. Li, S.K. Yang, X.X. Xu, W.P. Cai, Blue Luminescence of ZnO nanoparticles based on non-equilibrium processes: defect origins and emission controls, Adv. Funct. Mater. 20 (2010) 561–572, https://doi.org/10.1002/adfm.200901884.

[29] V. Srikant, D.R. Clarke, On the optical band gap of zinc oxide, J. Appl. Phys. 83 (1998) 5447–5451, https://doi.org/10.1063/1.367375.

[30] X.Y. Zhou, A.Q. Wang, Y. Wang, L.Z. Bian, Z.X. Yang, Y.Z. Bian, Y. Gong, X.F. Wu, N. Han, Y.F. Chen, Crystal-defect-dependent gas-sensing mechanism of the single ZnO nanowire sensors, ACS Sens. 3 (2018) 2385–2393, https://doi.org/10.1021/acssensors.8b00792.

[31] V. Siva, K. Park, M.S. Kim, Y.J. Kim, G.J. Lee, M.J. Kim, Y.M. Song, Mapping the structural, electrical, and optical properties of hydrothermally grown phosphorus-doped ZnO nanorods for optoelectronic device applications, Nanoscale Res. Lett. 14 (2019) 110, https://doi.org/10.1186/s11671-019-2920-3.

[32] S.M. Evans, N.C. Giles, L.E. Halliburton, L.A. Kappers, Further characterization of oxygen vacancies and zinc vacancies in electron-irradiated ZnO, J. Appl. Phys. 103 (2008) 043710, , https://doi.org/10.1063/1.2833432.

[33] X.J. Wang, L.S. Vlasenko, S.J. Pearton, W.M. Chen, I.A. Buyanova, Oxygen and zinc vacancies in as-grown ZnO single crystals, J. Phys. D: Appl. Phys. 42 (2009) 175411, , https://doi.org/10.1088/0022-3727/42/17/175411.

[34] B. Schallenberger, A. Hausmann, Eigenstörstellen in elektronenbestrahltem Zinkoxid, Zeitschrift für Physik B Condensed Matter 23 (1976) 177–181, https://doi.org/10.1007/BF01352713.

[35] V. Soriano, D. Galland, Photosensitivity of the EPR spectrum of the F^+ center in ZnO, Phys. Status Solidi B 77 (1976) 739–743, https://doi.org/10.1002/pssb.2220770239.

[36] M.S. Holston, E.M. Golden, B.E. Kananen, J.W. McClory, N.C. Giles, L.E. Halliburton, Identification of the zinc-oxygen divacancy in ZnO crystals, J. Appl. Phys. 119 (2016) 145701, , https://doi.org/10.1063/1.4945703.

[37] S. Pal, T. Rakshit, S.S. Singha, K. Asokan, S. Dutta, D. Jana, A. Sarkar, Shallow acceptor state in ZnO realized by ion irradiation and annealing route, J. Alloys Compd. 703 (2017) 26–33, https://doi.org/10.1016/j.jallcom.2017.01.331.

[38] V. Prozheeva, K.M. Johansen, P.T. Neuvonen, A. Zubiaga, L. Vines, A.Y. Kuznetzov, F. Tuomisto, Subsurface damage in polishing–annealing processed ZnO substrates, Mater. Sci. Semicond. Process. 69 (2017) 19–22, https://doi.org/10.1016/j.mssp.2017.02.021.

[39] Y.K. Frodason, K.M. Johansen, A. Alkauskas, L. Vines, Negative-U and polaronic behavior of the Zn-O divacancy in ZnO, Phys. Rev. B 99 (2019) 174106, , https://doi.org/10.1103/PhysRevB.99.174106.

[40] J. Bang, Y.S. Kim, C.H. Park, F. Cao, S.B. Zhang, Understanding the presence of vacancy clusters in ZnO from a kinetic perspective, Appl. Phys. Lett. 104 (2014) 252101, , https://doi.org/10.1063/1.4884653.

[41] D. Galland, A. Herve, ESR spectra of the zinc vacancy in ZnO, Phys. Lett. A 33 (1970) 1–2, https://doi.org/10.1016/0375-9601(70)90614-6.

[42] A.L. Taylor, G. Filipovich, G.K. Lindeberg, Electron paramagnetic resonance associated with Zn vacancies in neutron-irradiated ZnO, Solid State Commun. 8 (1970) 1359–1361, https://doi.org/10.1016/0038-1098(70)90042-6.

[43] K. Tang, S.M. Zhu, Z.H. Xu, Y. Shen, J.D. Ye, S.L. Gu, Formation of V_{Zn}-N_O acceptors with the assistance of tellurium in nitrogen-doped ZnO films, J. Alloys Compd. 699 (2017) 484–488, https://doi.org/10.1016/j.jallcom.2016.12.395.

[44] D.B. Wang, S.J. Jiao, S. Zhang, H.L. Li, S.Y. Gao, J.Z. Wang, J.X. Ren, Q.J. Yu, Y. Zhang, Growth mechanism and optical properties of phosphorus-doped ZnO nanorods synthesized by hydrothermal method, Phys. Status Solidi A 214 (2017) 1600959, https://doi.org/10.1002/pssa.201600959.

[45] Y.R. Ryu, T.S. Lee, H.W. White, Properties of arsenic-doped p-type ZnO grown by hybrid beam deposition, Appl. Phys. Lett. 83 (2003) 87–89, https://doi.org/10.1063/1.1590423.

[46] C.Q. Luo, L.P. Ho, F. Azad, W. Anwand, M. Butterling, A. Wagner, A. Kuznetsov, H. Zhu, S.C. Su, F.C.C. Ling, Sb-related defects in Sb-doped ZnO thin film grown by pulsed laser deposition, J. Appl. Phys. 123 (2018) 161525, , https://doi.org/10.1063/1.4997510.

[47] M.R. Wagner, G. Callsen, J.S. Reparaz, J.H. Schulze, R. Kirste, M. Cobet, I.A. Ostapenko, S. Rodt, C. Nenstiel, M. Kaiser, A. Hoffmann, A.V. Rodina, M.R. Phillips, S. Lautenschläger, S. Eisermann, B.K. Meyer, Bound excitons in ZnO: structural defect complexes versus shallow impurity centers, Phys. Rev. B 84 (2011) 035313, , https://doi.org/10.1103/PhysRevB.84.035313.

[48] C. Bazioti, A. Azarov, K.M. Johansen, B.G. Svensson, L. Vines, A.Y. Kuznetsov, Ø. Prytz, Role of nitrogen in defect evolution in zinc oxide: STEM–EELS nanoscale investigations, J. Phys. Chem. Lett. 10 (2019) 4725–4730, https://doi.org/10.1021/acs.jpclett.9b01472.

[49] F.X. Xiu, Z. Yang, L.J. Mandalapu, D.T. Zhao, J.L. Liu, Photoluminescence study of Sb-doped p-type ZnO films by molecular-beam epitaxy, Appl. Phys. Lett. 87 (2005) 252102, , https://doi.org/10.1063/1.2146208.

[50] L.L. Shi, L.C. Du, Y.T. Xu, L. Jin, H. Zhang, Y. Li, X.H. Ma, Y.G. Zou, D.X. Zhao, Morphology and electrical characteristics of p-type ZnO microwires with zigzag rough surfaces induced by Sb doping, RSC Adv. 8 (2018) 35023–35030, https://doi.org/10.1039/C8RA07135G.